Energy- and angle-resolved pump–probe femtosecond photoelectron spectroscopy: Molecular rotation

Yasuki Arasaki and Kazuo Takatsuka[a)]
Department of Basic Science, Graduate School of Arts and Sciences, University of Tokyo, Komaba, 153-8902, Tokyo, Japan

Kwanghsi Wang and Vincent McKoy
Laboratory for Molecular Sciences, California Institute of Technology, Pasadena, California 91125

(Received 6 December 2000; accepted 13 February 2001)

We have incorporated a classical treatment of molecular rotation into our formulation of energy- and angle-resolved pump–probe photoelectron spectroscopy. This classical treatment provides a useful approach to extracting the photoelectron signal primarily associated with vibrational dynamics in cases where rotational motion is slow and the coupling between rotational and vibrational motion is weak. We illustrate its applicability with pump–probe photoelectron spectra for wave packets on the $^1\Sigma_u^+$ double-minimum state of Na_2. © *2001 American Institute of Physics.*
[DOI: 10.1063/1.1361067]

I. INTRODUCTION

Femtosecond time-resolved spectroscopy has been widely exploited in numerous applications ranging from fundamental studies of real-time motion in the photodissociation of NaI to studies of electron transfer.[1–3] In this spectroscopy, a femtosecond pulse (pump) is used to launch a wave packet onto a state where it evolves in accordance with the time scales for vibrational ($\sim 10^{-13}$ s) and rotational ($\sim 10^{-10}$ s) motion. The evolution of the wave packet is monitored by time-delayed femtosecond excitation to a higher electronic state which serves as a template. Various techniques including absorption, laser-induced fluorescence, multiphoton ionization, photoelectron spectroscopy, time-resolved mass spectroscopy, and stimulated emission pumping have been used to probe these wave packets.[2–8]

Time-resolved ionization offers several advantages as a probe of these wave packets.[5,9–11] For example, the ground state of an ion is often more readily characterized than higher excited states of the molecule. Ionization also provides ions and photoelectrons and while ion detection provides mass and kinetic-energy resolution, pump–probe photoelectron spectra are well suited for monitoring wave packet dynamics and the evolution of electronic structure along all energetically allowed internuclear distances simultaneously.[5–8] This advantage of time-resolved photoelectron spectroscopy has already been well demonstrated in the picosecond domain.[12–14] Its potential for probing molecular dynamics in the femtosecond regime has also been exploited experimentally for several systems.[5–7,15] Furthermore, Davies *et al.*[8] have recently reported results of the first femtosecond photoelectron-photoion coincidence imaging studies of photodissociation dynamics.

Efforts to map vibrational wave packets with the help of femtosecond pump–probe techniques and energy-resolved photoelectron spectra were stimulated by the early studies of Seel and Domcke[16] and of Engel, Meier, and Braun[17] who showed how the dynamics of a vibrational wave packet, including its reflection and splitting at a potential barrier, can be seen in the time-dependent photoelectron energy distribution. This was nicely illustrated for the case of wave packet motion on the $^1\Sigma_u^+$ double-minimum potential of Na_2 that arises from the avoided crossing of two diabatic states. While these early studies served to illustrate the utility and promise of pump–probe photoelectron spectroscopy for real-time mapping of wave packet dynamics, they generally did not account for the dependence of the underlying photoionization amplitudes on geometry. Engel and co-workers, in fact, noted that the assumption of a position-independent transition dipole was questionable in cases where wave packets moved through regions of avoided crossings and over rather large distances.[17]

In recent papers[18–21] we presented results of our studies of energy- and angle-resolved photoelectron spectra for femtosecond pump–probe ionization of wave packets in the $^1\Sigma_u^+$ double-minimum state in Na_2 molecules aligned by a linearly polarized pulse. These studies employed geometry- and energy-dependent photoelectron matrix elements derived from sophisticated descriptions of the wave functions for the double-minimum state and for the molecular photoelectrons. We reported spectra for molecules aligned by a linearly polarized pulse and ionized by a probe pulse polarized either parallel or perpendicular to the pump pulse. These studies illustrated some important points: First, a robust description of the photoionization amplitudes can enhance the utility of femtosecond photoelectron spectroscopy as a probe of wave packet motion[17] and of the evolution of electronic structure. In fact, this is particularly true when the wave packet moves through an avoided crossing. Second, photoelectron angular distributions are insightful fingerprints of vibrational wave packet dynamics.

In these studies, however, we assumed that the molecule

a)Electronic mail: KazTak@mns2.c.u-tokyo.ac.jp

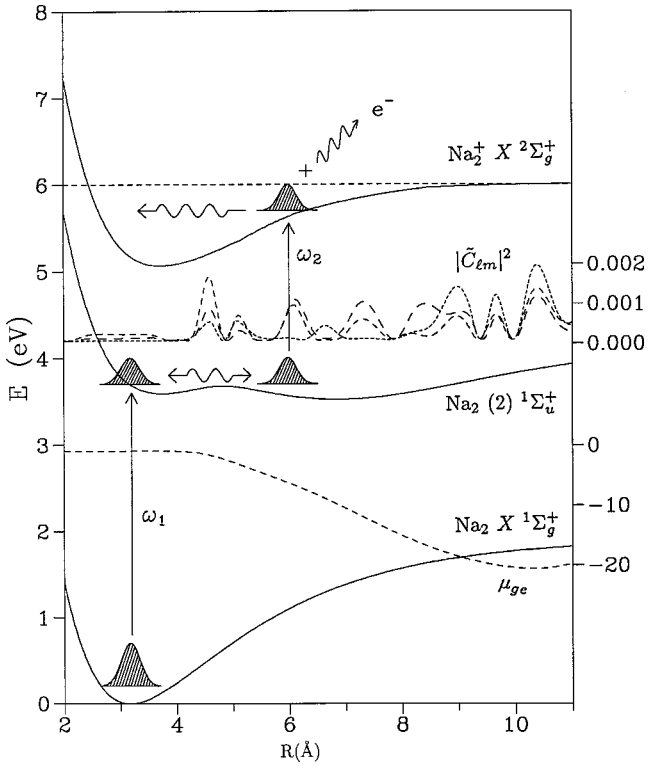

FIG. 1. Potential curves for the $X\ ^1\Sigma_g^+$ and (2) $^1\Sigma_u^+$ states of Na_2 and the $X\ ^2\Sigma_g^+$ state of Na_2^+. The dipole amplitude (μ_{ge}) and photoionization coefficients ($\tilde{C}_{lm}$) for the molecule parallel to the pump and probe fields are also shown for a kinetic energy of 0.5967 eV. The partial waves $l=0$, 2, and 4 with $m=0$ are denoted by long, medium, and short dashed lines, respectively.

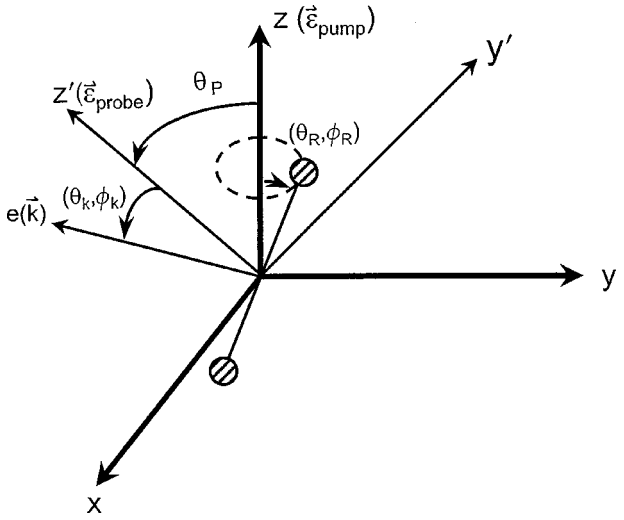

FIG. 2. Orientation of the molecule and pump and probe laser fields: molecular orientation angles (θ_R,ϕ_R) are specified in the pump frame and photoelectron angles (θ_k,ϕ_k) in the probe frame.

did not rotate but remained fixed in space with its axis aligned along the polarization vector of the pump laser.[18–21] The probe pulse was then assumed to be either parallel or perpendicular to the molecular axis. While this assumption may be appropriate for rotationally cold systems, it is of interest to examine how these photoelectron spectra may be influenced by molecular rotation. Although our formulation of energy- and angle-resolved pump–probe photoelectron spectra can account for quantum molecular rotation,[18] the computational effort escalates if rotation is included. In those cases where coherent interactions among vibrational and rotational modes are not large, which we assume here, a classical treatment of molecular rotation is a practical and useful first step in exploring the influence of molecular rotation on these pump–probe photoelectron spectra. In this paper, we employ our formulation of pump–probe photoelectron spectra and a classical model of rotation to explore the effects of rotation on such spectra. Results of applications to photoelectron spectra for wave packets on the double-minimum state of Na_2 are presented.

II. PUMP–PROBE PHOTOELECTRON SPECTROSCOPY: FORMULATION

Figure 1 illustrates some key features of our pump–probe femtosecond photoelectron spectroscopy scheme. Application of this scheme to the probing of the vibrational dynamics on the $^1\Sigma_u^+$ double-minimum state of the Na_2 molecule by energy- and angle-resolved time-dependent photoelectron spectra has been described in detail in a previous paper.[19] Here we briefly review the general formulation employed in those studies, with some emphasis on the coordinate frames used in describing molecular orientation.

A linearly polarized pulse of frequency ω_1 prepares a wave packet in the double-minimum $^1\Sigma_u^+$ state which is then ionized by a time-delayed linearly polarized pulse of frequency ω_2. The polarized pump pulse produces an aligned distribution of Na_2 molecules since only those molecules with their transition moments parallel or nearly parallel to the polarization vector of the pump pulse are excited. The dynamics of the system is monitored through the energy and angular distributions of photoelectrons produced from ionization of the wave packet for various pump–probe delay times.

The orientation of the molecule and pump and probe laser fields is shown in Fig. 2. Three coordinate frames naturally arise in this picture. Since the pump pulse prepares an aligned distribution of molecules, the time-dependent molecular orientation $\hat{R}=(\theta_R,\phi_R)$ is best defined in the pump frame (X,Y,Z), where the Z-axis lies in the direction of the pump polarization. The probe polarization vector defines the Z'-axis of the probe frame (X',Y',Z') in which it is most convenient to define the photoelectron detection angle (θ_k,ϕ_k). The molecule field interaction is best described in the molecular body frame (x,y,z). Without loss of generality, the probe polarization vector can be assumed to lie on the XZ-plane so that a single angle θ_P conveniently describes the relative orientations of pump and probe. Taking the probe frame Y'-axis to coincide with the pump frame Y-axis unambiguously orients the probe frame relative to the pump frame.

The time-dependent wave function for this system can be written as

$$\Psi(\mathbf{r},\mathbf{R},t)=\chi_g(\mathbf{R},t)\Phi_g(\mathbf{r};R)+\chi_e(\mathbf{R},t)\Phi_e(\mathbf{r};R)+\int d\mathbf{k}\chi_{\mathbf{k}}(\mathbf{R},t)\Phi_{\mathbf{k}}^{(-)}(\mathbf{r};R), \quad (1)$$

where Φ_g, Φ_e, and $\Phi_{\mathbf{k}}^{(-)}$ are the electronic eigenfunctions for the ground, excited, and final ionized adiabatic states, respectively, χ_g, χ_e, and $\chi_{\mathbf{k}}$ are nuclear wave packets on the respective potential curves, $\mathbf{r}$ denotes electronic coordinates, and $\boldsymbol{k}$ the wave vector of the photoelectron. The nuclear coordinate $\mathbf{R}=(R,\hat{R})$, with R the internuclear distance, describes both vibrational and rotational motion. The interaction between the molecule and the laser fields is given by

$$V(t)=V_1(t)+V_2(t;\Delta T)=E_{01}f_1(t)\sin(\omega_1 t)\boldsymbol{\epsilon}_{\text{pump}}\cdot\mathbf{d}+\tfrac{1}{2}E_{02}f_2(t-\Delta T)\times\exp(-i\omega_2(t-\Delta T))\boldsymbol{\epsilon}_{\text{probe}}\cdot\mathbf{d}, \quad (2)$$

where E_{01} and E_{02} are the field amplitudes, $f_1(t)$ and $f_2(t-\Delta T)$ are the pulse envelope functions with ΔT the time delay between the two pulses, $\boldsymbol{\epsilon}_{\text{pump}}$ and $\boldsymbol{\epsilon}_{\text{probe}}$ the polarization vectors, and $\mathbf{d}$ the electric dipole operator. Centers of the envelope functions for the pump and probe pulses are at $t=0$ and $t=\Delta T$, respectively, and are taken here to be Gaussian functions although the theory is general.

Equations (1) and (2) yield the equations of motion for the nuclear wave packets,

$$i\hbar\frac{\partial}{\partial t}\chi_g(\mathbf{R},t)=[T_N+V_g(R)]\chi_g(\mathbf{R},t)+\langle\Phi_g(R)|V_1(t)|\Phi_e(R)\rangle\chi_e(\mathbf{R},t), \quad (3)$$

$$i\hbar\frac{\partial}{\partial t}\chi_e(\mathbf{R},t)=[T_N+V_e(R)]\chi_e(\mathbf{R},t)+\langle\Phi_e(R)|V_1(t)|\Phi_g(R)\rangle\chi_g(\mathbf{R},t)+\int dk\langle\Phi_e(R)|V_2(t;\Delta T)|\Phi_{\mathbf{k}}^{(-)}(R)\rangle\times\chi_{\mathbf{k}}(\mathbf{R},t), \quad (4)$$

and

$$i\hbar\frac{\partial}{\partial t}\chi_{\mathbf{k}}(\mathbf{R},t)=\left[T_N+V_{\text{ion}}(R)+\frac{(k\hbar)^2}{2m_e}\right]\chi_{\mathbf{k}}(\mathbf{R},t)+\langle\Phi_{\mathbf{k}}^{(-)}(R)|V_2(t;\Delta T)|\Phi_e(R)\rangle\chi_e(\mathbf{R},t), \quad (5)$$

where $V_g(R)$, $V_e(R)$, and $V_{\text{ion}}(R)$ are the ground, excited, and ion potential curves, and m_e denotes the electron mass.

To proceed one requires the interaction matrix elements between the ground and excited state (V_1) and between the excited and ionized state (V_2). The interaction matrix element between the ground and excited states is given by

$$V_{eg}(R)=\langle\Phi_e(R)|V_1(t)|\Phi_g(R)\rangle=E_{01}f_1(t)\sin(\omega_1 t)d_{eg}(R)\cos(\theta_R), \quad (6)$$

where d_{eg} is the magnitude of the transition moment between the ground and excited states and θ_R is the angle between the molecular axis and the pump polarization. To obtain the matrix element between the excited and ionized states, $\langle\Phi_k^{(-)}(R)|V_2(t-\Delta T)|\Phi_e(R)\rangle$, we write $\Phi_{\mathbf{k}}^{(-)}$ as an antisymmetrized product of an ion wave function, Φ_+, and a photoelectron orbital, $\phi_{\mathbf{k}}^{(-)}$,

$$\Phi_{\mathbf{k}}^{(-)}=\mathcal{A}(\Phi_+\cdot\phi_{\mathbf{k}}^{(-)}), \quad (7)$$

where

$$\phi_{\mathbf{k}}^{(-)}=\sum_{l,m,\lambda} i^l e^{-i\eta_l}\mathcal{D}_{\lambda m}^{l}(\hat{R}')Y_{lm}^{*}(\hat{k})\psi_{kl\lambda}^{(-)}(\mathbf{r}';R), \quad (8)$$

with $\mathbf{r}'$ being the electronic coordinate vector in the molecular frame. In Eq. (8) $\psi_{kl\lambda}^{(-)}$ is a partial-wave component of the photoelectron orbital in the molecular frame with momentum $\mathbf{k}$, λ is the projection of l in the molecular frame, $\mathcal{D}_{\lambda m}^{l}$ transforms the molecular-frame wave functions to those in the laboratory (probe) frame, and η_l is the Coulomb phase shift.[22] Photoelectron detection will be assumed to be relative to the polarization vector of the probe laser. The dipole operator is hence given by

$$D_{\mu_0}=\sqrt{\frac{4\pi}{3}}r\sum_{\mu}\mathcal{D}_{\mu\mu_0}^{1}(\hat{R}')Y_{1\mu}(\hat{r}') \quad (9)$$

in the probe laser frame. The interaction V_2 between the probe laser and the molecule becomes

$$V_2=\tfrac{1}{2}E_{02}\cdot f_2(t-\Delta T)\exp(-i\omega_2(t-\Delta T))D_{\mu_0}, \quad (10)$$

and the coupling matrix element between the excited state Φ_e and the final ionized state can be written as

$$V_{ie}(R)=\langle\Phi_{\mathbf{k}}^{(-)}(R)|V_2(t;\Delta T)|\Phi_e(R)\rangle=\tfrac{1}{2}E_{02}\cdot f_2(t-\Delta T)\exp(-i\omega_2(t-\Delta T))\times\sum_{lm}C_{lm}Y_{lm}(\hat{k}), \quad (11)$$

$$C_{lm}(k,R,\theta_R,\phi_R,\theta_P)=\sqrt{\frac{4\pi}{3}}\sum_{\lambda\mu}I_{l\lambda\mu}\mathcal{D}_{\lambda m}^{l*}(\hat{R}')\mathcal{D}_{\mu\mu_0}^{1}(\hat{R}'). \quad (12)$$

$I_{l\lambda\mu}$ is a partial-wave matrix element in the molecular frame. These are formed from dipole matrix elements between $|\Phi_+\psi_{kl\lambda}^{(-)}\rangle$ and the components of the CI wave function used to describe Φ_e. For the case of ionization of an orbital ϕ_i into $\psi_{kl\lambda}^{(-)}$ these assume the form

$$I_{l\lambda\mu}^{(0)}(R)=(-i)^l e^{i\eta_l}\sum_{l_0\lambda_0}\langle\psi_{kl\lambda}^{(-)}|rY_{1\mu}(\hat{r}')|\phi_{i,l_0\lambda_0}(r)Y_{l_0\lambda_0}(\hat{r}')\rangle. \quad (13)$$

The C_{lm} coefficients of Eq. (12) provide the underlying dynamical information needed to describe the photoionization of an oriented Na_2 molecule by the probe laser. The angular momentum coupling inherent in molecular photoelectrons can be seen in a single-center expansion of $\psi_{kl\lambda}$ for a linear molecule

$$\psi_{kl\lambda}^{(-)}(\mathbf{r},R)=\sum_{l'}g_{ll'\lambda}^{(-)}(k,r,R)Y_{l'\lambda}. \quad (14)$$

$\psi_{kl\lambda}^{(-)}$ are obtained numerically using a procedure outlined in detail elsewhere.[22] The Euler angles $\hat{R}'$ in Eqs. (9) and (12) are readily determined as a function of the angles θ_R, ϕ_R, and θ_P by considering the orientation of the body and probe frames to the pump frame (see the Appendix).

Expanding the ion nuclear wave packet $\chi_{\mathbf{k}}$ in partial waves about $\hat{k}$,

$$\chi_{\mathbf{k}}(\mathbf{R},t)=\sum_{lm}\chi_{klm}(\mathbf{R},t)Y_{lm}(\hat{k}), \tag{15}$$

and using Eqs. (6) and (11), the equations of motion Eqs. (3)–(5) lead to

$$i\hbar\frac{\partial}{\partial t}\chi_g(\mathbf{R},t)=[T_N+V_g]\chi_g(\mathbf{R},t)+V_{ge}(t,\theta_R)\chi_e(\mathbf{R},t), \tag{16}$$

$$\begin{aligned}i\hbar\frac{\partial}{\partial t}\chi_e(\mathbf{R},t)=&[T_N+V_e]\chi_e(\mathbf{R},t)+V_{eg}(t,\theta_R)\chi_g(\mathbf{R},t)\\&+\frac{1}{2}\sum_{lm}\int dk k^2 E_{02}f_2(t-\Delta T)\\&\times\exp(i\omega_2(t-\Delta T))C_{lm}^*(k,R,\theta_R,\phi_R,\theta_P)\\&\cdot\chi_{klm}(\mathbf{R},t;\Delta T,\theta_P),\end{aligned} \tag{17}$$

and

$$\begin{aligned}i\hbar\frac{\partial}{\partial t}&\chi_{klm}(\mathbf{R},t;\Delta T,\theta_P)\\&=\left[T_N+V_{\text{ion}}+\frac{(k\hbar)^2}{2m_e}\right]\chi_{klm}(\mathbf{R},t;\Delta T,\theta_P)\\&\quad+\tfrac{1}{2}E_{02}f_2(t-\Delta T)\exp(-i\omega_2(t-\Delta T))\\&\quad\times C_{lm}(k,R,\theta_R,\phi_R,\theta_P)\cdot\chi_e(\mathbf{R},t).\end{aligned} \tag{18}$$

Discretization of the integration over k results in a set of coupled equations for χ_0, χ_e, and the set of $\{\chi_{k_j lm}\}$ for all l and m at each quadrature point k_j. Details of the procedures employed in solving these equations are given in Ref. 19.

III. CLASSICAL TREATMENT OF MOLECULAR ROTATION

These equations of motion are general enough to account for both molecular vibration and rotation quantum mechanically. For example, the nuclear wave packets, $\chi_{\hat{\mathbf{k}}}(\mathbf{R},t)$, can be expanded in rotational wave functions $\Theta_{LM}(\hat{R})$

$$\chi_{\mathbf{k}}(\mathbf{R},t)=\sum_{L,M}\chi_{\mathbf{k},LM}(R,t)\Theta_{LM}(\hat{R}), \tag{19}$$

and a coupled set of equations of motion can be formulated for the $\chi_{\mathbf{k},LM}(R,t)$. Here L and M are, respectively, the rotational quantum number and its projection onto, for instance, the pump polarization. While coherent interactions among rotational levels and rotational-vibrational levels can be important in angle-resolved photoelectron spectra for light molecules or rotationally hot systems, we nonetheless assumed in our previous study that the molecule did not rotate significantly on the vibrational time scale.[19] We made this assumption for several reasons. First, our interest lies primarily in using these time-resolved photoelectron spectra as a probe of dynamics in regions of nondiabatic behavior between electronic states. Second, this is a good assumption for rotationally cold levels where the rotational time scale may be orders of magnitude larger than the time scale for vibrations. Finally, inclusion of rotational states would result in a dramatic increase in the number of channels and in the computational effort required for the solution of the resulting equations. On the other hand, for a molecule with fixed orientation, the coupled equations need only describe the vibrational wave packets.

As a first step in exploring how these pump–probe photoelectron spectra are influenced by rotation, we employ a classical model. We assume that molecular rotation is slow and explicitly account for it by changing the molecular orientation with pump–probe delay time. This procedure requires that the C_{lm} coefficients of Eq. (12) be calculated for every delay time but does not significantly increase the overall computational effort.

Although our formulation is general enough to provide photoelectron distributions for arbitrary molecular orientations and planes of detection, the symmetry of the excited state studied here should result in a strong signal in the XZ-plane for a perpendicular orientation of the probe laser and molecular axis. We hence assume here that the molecule rotates in the XZ-plane, the plane containing the polarization vectors of the pump and probe lasers, at a constant angular velocity and that photoelectrons are also detected in the XZ-plane. Furthermore, this treatment assumes that molecular rotation is dynamically uncoupled from vibrational motion. This can clearly not be a good approximation in cases where the bond length changes significantly during rotation since in such cases there can be exchange of energy between rotational and vibrational modes. When pumped to an energy above the potential barrier separating the inner and outer wells, motion on the double-minimum state of Na_2 is just such a case as the bond stretches from about 3 Å to 10 Å. Nonetheless, we study this case simply to explore pump–probe photoelectron spectra of a rotating molecule rather than as a simulation of a real system.

A. Vibrational wave packets on the excited state

Figure 3 shows the behavior of vibrational wave packets prepared by two different pump photons. The left panel, (a), shows the wave packet for a pump photon of 3.600 eV while the right panel, (b), shows the wave packet for a pump photon of 3.676 eV. In both cases the full width at half maximum (FWHM) is 120 fs. In the lower energy case, (a), the wave packet does not have enough energy to move beyond the potential barrier and remains in the inner well, oscillating between 3.5 Å and 4.0 Å with a vibrational frequency of about 340 fs. For the higher energy pump photon, case (b), the energy lies at the top of the barrier between the two wells and at the barrier the wave packet splits into a lower energy component that remains in the inner well and a higher energy component that travels out to the outer well. At 605 fs after

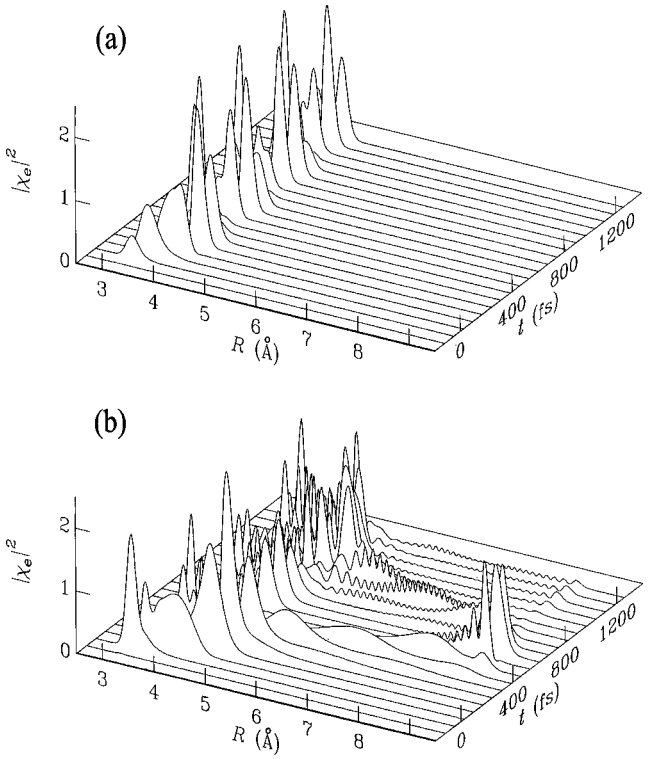

FIG. 3. Time evolution of the absolute square of the excited state wave packets for (a) pump energy $\hbar\omega_1 = 3.600$ eV and (b) $\hbar\omega_1 = 3.676$ eV.

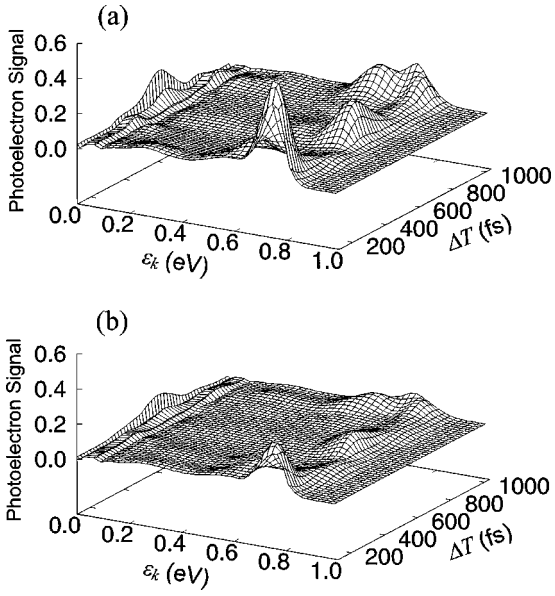

FIG. 4. Photoelectron signal $P(\epsilon_k)$ vs kinetic energy and delay time. The photon energy of the pump laser is $\hbar\omega_1 = 3.676$ eV. The polarization vector of the probe laser is set parallel (a) and perpendicular (b) to that of the pump laser.

the pump pulse, the wave packet is peaked near 4.4 Å around the potential barrier and at 8.7 Å, the outer turning points of the wells. The longer vibrational period is 1 ps.

B. Dependence of energy- and angle-resolved photoelectron spectra on molecular vibration and rotation

1. Photoelectron energy distribution versus vibrational motion

Photoelectron energy distributions as a function of pump–probe delay time are a sensitive probe of the motion of a vibrational wave packet. Studies by Engel and co-workers[17] were the first to illustrate how well suited pump–probe energy-resolved photoelectron spectra are for monitoring the evolution of a vibrational wave packet with internuclear distance in real time. These studies, however, generally assumed a constant value for the photoionization amplitude as a function of internuclear distance and their calculated spectra are hence essentially those expected within the Franck–Condon approximation. Engel and co-workers[17] also noted that such an assumption would be obviously questionable for wave packet motion through regions of avoided crossings, where the electronic wave function evolves rapidly with internuclear distance, or when wave packets move over large distances. We have recently reported results of studies of the pump–probe photoelectron spectra for wave packet motion on the $^1\Sigma_u^+$ double-minimum state arising from an avoided crossing of two diabatic states.[19] These studies employed geometry-dependent photoionization amplitudes. To put our present work into context, it is helpful to reproduce some of these results here. Our photoelectron energy distributions are defined as

$$P(\epsilon_k;\Delta T,\theta_R,\theta_P)=\sum_{lm} k\int dR|\chi_{klm}(R,t_f;\Delta T,\theta_R,\theta_P)|^2, \tag{20}$$

where ϵ_k is the photoelectron energy, ΔT is the pump–probe delay time, and θ_R and θ_P orient the molecular axis and the probe polarization, respectively (Fig. 1). The signal is extracted a long time, t_f, after the probe pulse has been turned off. Figure 4(a) shows these photoelectron energy distributions for a pump photon of 3.676 eV [top of barrier case of Fig. 3(b)], a probe photon of 2.278 eV, and both θ_R and θ_P set to zero. This corresponds to fixing the molecule in space with its molecular axis parallel to the pump polarization. These spectra display the sensitivity of the kinetic energy distribution to the vibrational wave packet and to the changes of the photoionization amplitudes with internuclear distance.

2. Kinetic energy distribution versus molecular orientation

Figure 4(b) shows the photoelectron kinetic energy distribution when the molecule is held fixed at $\theta_R = 0$ and the probe polarization is perpendicular to the molecular axis ($\theta_R = \pi/2$). The global features of the kinetic energy distributions for the probe polarization perpendicular to the molecular axis are similar to those for the probe polarization parallel to the molecular axis except for a noticeable difference in the magnitudes of the signal.

3. Photoelectron angular distribution versus molecular vibration

The photoelectron angular distributions, integrated over kinetic energy, are given by

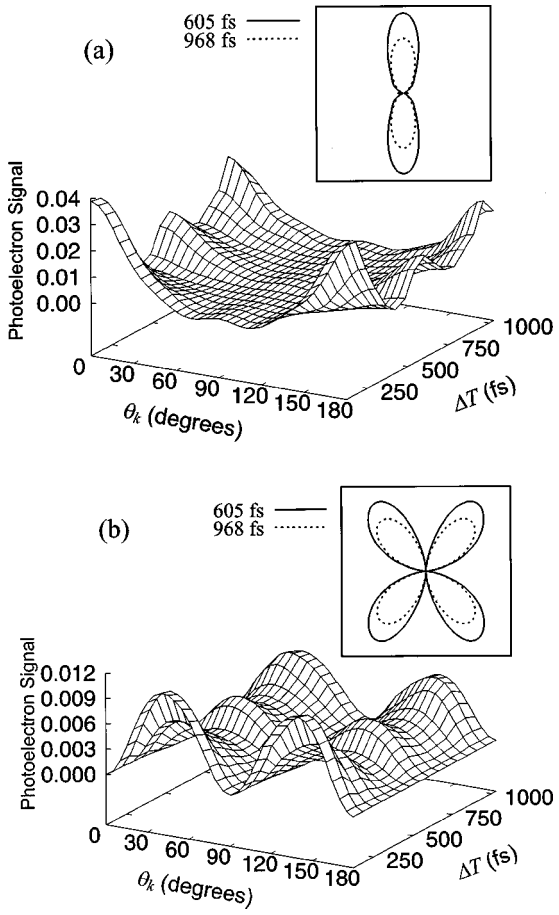

FIG. 5. The photoelectron angular distributions as a function of delay time. As in Fig. 4, the photon energy of the pump laser is $\hbar\omega_1 = 3.6763$ eV. The polarization vector of the probe laser is set parallel (a) and perpendicular (b) to that of the pump laser. The insets show a polar coordinate representation of $A(\theta_k, \Delta T)$ at $\Delta T = 605$ fs (smooth lines) and $\Delta T = 968$ fs (broken curves).

$$A(\theta_k;\Delta T,\theta_R,\theta_P) = \int dk k^2 \int dR \left| \sum_{lm} \chi_{klm}(R,t_f;\Delta T,\theta_R,\theta_P) Y_{lm}(\theta_k,\phi_k) \right|^2 . \tag{21}$$

Figure 5(a) shows these energy-integrated photoelectron angular distributions as a function of pump–probe delay time, ΔT, for $\theta_R = \theta_P = 0$, i.e., pump and probe polarizations parallel to the molecular axis. Although their magnitude varies with pump–probe delay time, these energy-integrated angular distributions are basically d_{z^2}-like for all ΔT or different internuclear distances. It is worth noting here, however, that the energy-resolved photoelectron angular distributions do show variations with pump–probe delay time which reflect the evolution of electronic structure and photoionization dynamics.[21]

Figure 6 shows the $l=0$ and $l=2$ components of the ion wave packet [χ_{klm} of Eq. (16)] for a pump–probe delay of 605 fs and pump and probe photons of 3.6763 eV and 2.278 eV, respectively. For convenience, these figures only include contributions with energy less than 0.1 eV. These partial wave ion packets reflect the photoionization dynamics and

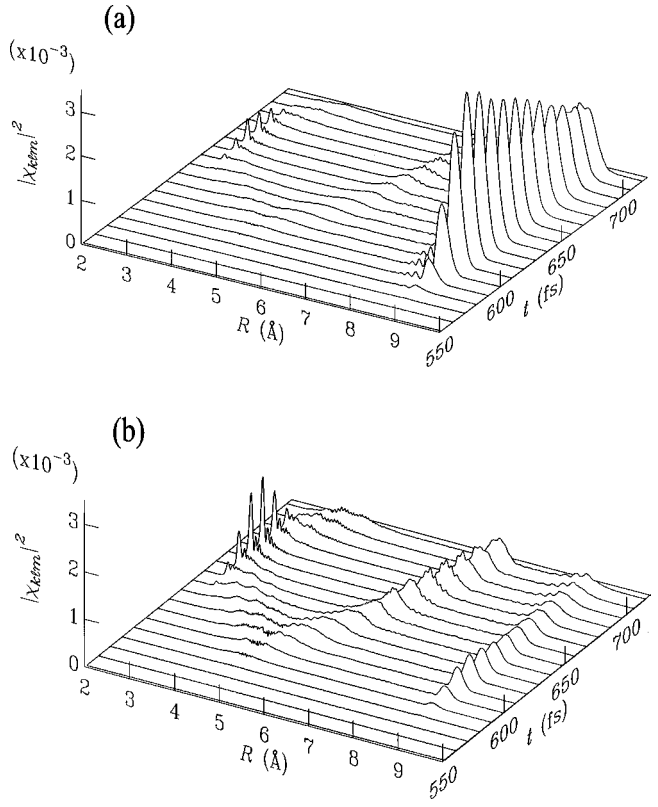

FIG. 6. Time evolution of resulting ion wave function components with photoelectron kinetic energy $\epsilon_k < 0.1$ eV and (a) $l=0$, and (b) $l=2$. As in Fig. 4, the photon energy of the pump laser is $\hbar\omega_1 = 3.6763$ eV. The polarization vector of the probe laser is set parallel to that of the pump laser.

may be useful maps of wave packet behavior in molecular systems.

4. Photoelectron angular distributions versus molecular orientation

The dependence of the photoelectron angular distributions on molecular orientation can be seen in Figs. 5(a) and 5(b) where we show these distributions for the probe polarization parallel and perpendicular to the molecular axis. Not surprisingly, these distributions have d_{z^2}-character for a parallel arrangement of the probe and molecular axis and d_{xz}-character when they are perpendicular. Such dependence of the angular distributions on relative orientation of the probe and molecule can be useful in real-time monitoring of molecular rotation.

IV. PHOTOELECTRON ANGULAR DISTRIBUTIONS FROM A ROTATING MOLECULE

A. Distributions from a rigid rotor

Before discussing the photoelectron spectra from a classically rotating Na_2, we examine the dependence of the photoionization amplitude squares [see Eq. (11)], i.e.,

$$\left| \sum_{lm} C_{lm} Y_{lm}(\theta_k,\phi_k) \right|^2 \tag{22}$$

for a rigid Na_2 rotor at specific internuclear distances and for different relative orientations of the molecular axis and probe polarization. The rows of Fig. 7 show the angular distribu-

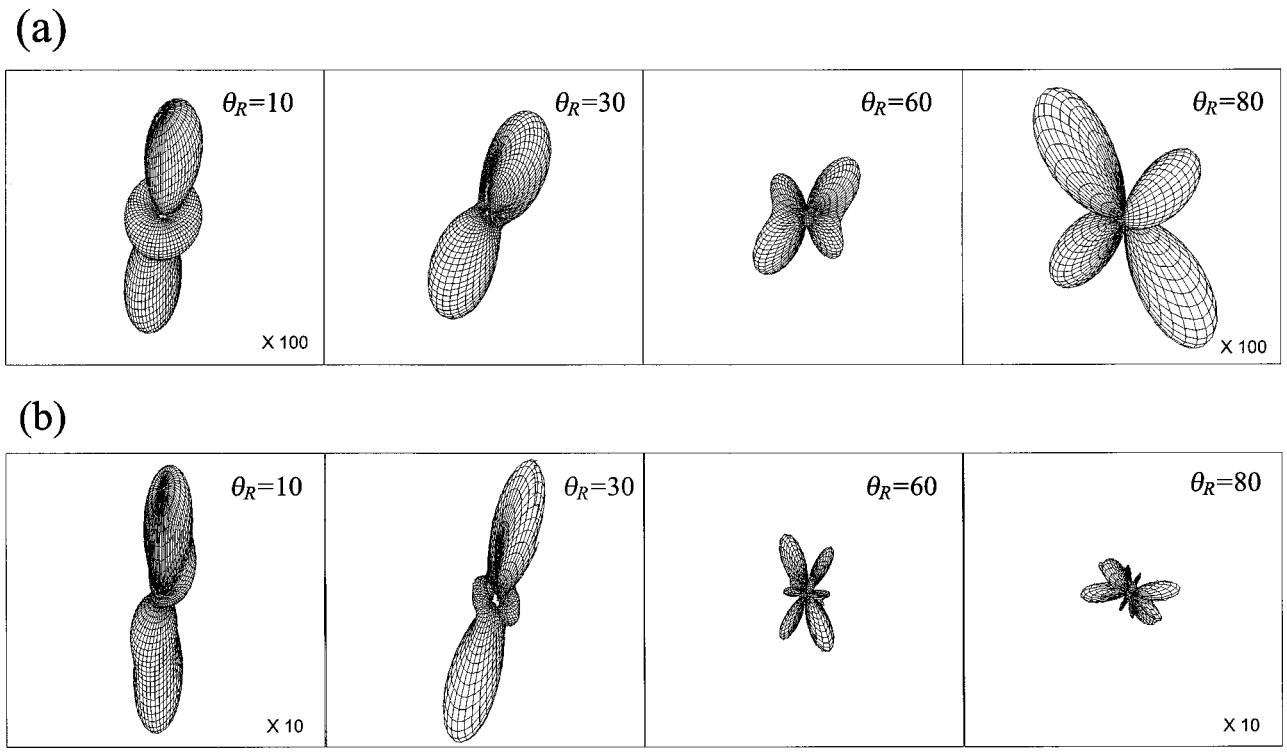

FIG. 7. Spatial distributions of photoionization amplitudes $|\Sigma_{lm}C_{lm}Y_{lm}(\theta_k,\phi_k)|^2$ for a photoelectron energy of 0.7689 eV at bond length of (a) 3 Å and (b) 9 Å.

tions for Na_2 tilted 10, 30, 60, and 80 deg away from the probe in the XZ-plane for internuclear distances of 3.0 Å and 9.0 Å and a photoelectron energy of 0.7689 eV. At the shorter of these distances, the spatial distribution has d_{z^2} character at a low angle of tilt and d_{xz} character at a large angle of tilt. At the larger internuclear distance of 9.0 Å the angular distributions reveal features arising from higher l-components.

B. Convolution of molecular vibration and rotation

We now examine the pump–probe spectra for a rotating Na_2 molecule assuming a classical model, as outlined in Sec. III, and that the molecule rotates in the XZ-plane with a period of 4080 fs. This assumption would best apply to rotationally cold molecules where the distribution of angular frequencies over the classical rotators may be expected to be very narrow. More generally, however, the photoelectron spectrum at a given delay time would reflect the distribution of angular frequencies among the rotors. For a period of 4080 fs, in the time it takes the molecule to rotate 90° from a parallel to a perpendicular orientation relative to the probe polarization, the inner-well wave packet component executes about three vibrational periods while the outer well component completes a single period. The rotation angle θ_R (in degrees) is related to the delay time, ΔT, via $\theta_R(\Delta T) = 0.088\,24\Delta T$.

Figure 8 shows these photoelectron energy distributions as a function of delay time for pump photon energies of 3.600 eV (inner well) and 3.676 eV (top of barrier), a probe pulse of 2.278 eV and for the molecular axis parallel to the probe polarization ($\theta_P = 0$). As discussed above, the overall shape of these photoelectron energy distributions does not depend much on the relative orientation of the molecular axis and probe polarization and hence the effect of rotation is not immediately apparent in either of these two cases. For the lower energy photon, case (a), evidence of the region of depleted photoionization amplitudes near 4 Å is apparent and the spectrum reflects the vibrational motion quite nicely. The peak around $\Delta T = 1020$ fs is slightly higher than the others,

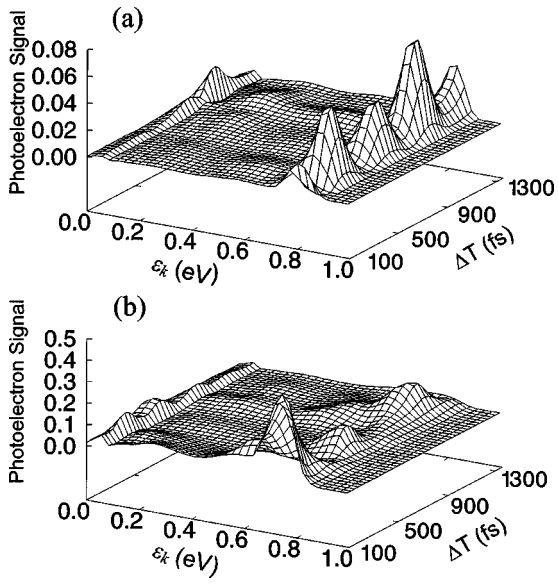

FIG. 8. Photoelectron kinetic energy distribution $P(\epsilon_k,\Delta T)$ for (a) pump energy $\hbar\omega_1 = 3.600$ eV and (b) $\hbar\omega_1 = 3.676$ eV.

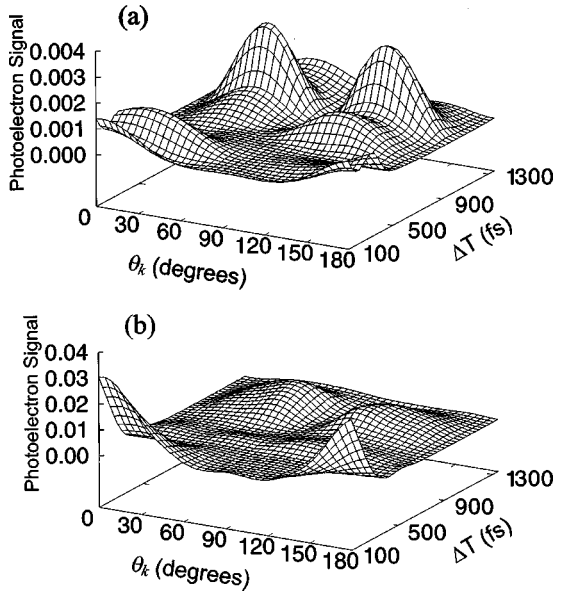

FIG. 9. Photoelectron angular distribution $A(\theta_k,\Delta T)$ in the XZ-plane ($\phi_k=0$) for (a) pump energy $\hbar\omega_1=3.600$ eV and (b) $\hbar\omega_1=3.676$ eV.

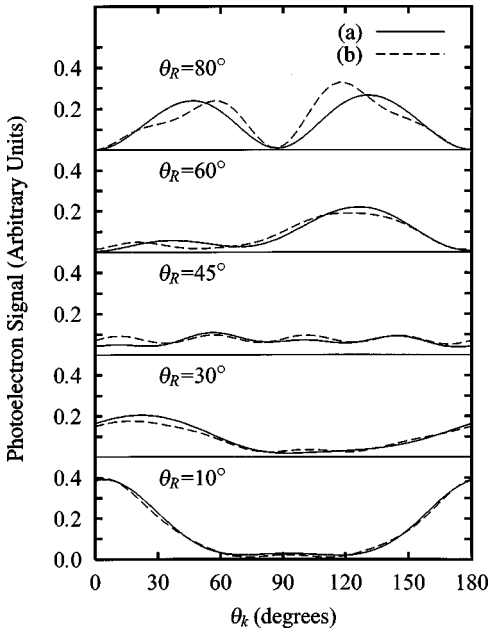

FIG. 10. Angular distribution $A(\theta_k,\theta_R)$ divided by total ion signal for (a) pump energy $\hbar\omega_1=3.600$ eV and (b) $\hbar\omega_1=3.676$ eV. $\phi_k=0$ as in Fig. 9.

since ionization is somewhat larger for a perpendicular orientation for the lower pump energy.

In the case of the larger pump photon energy, the photoelectron spectra are a bit more complex since the wave packet samples the oscillating photoionization amplitudes as it executes its large amplitude motion. The higher photoelectron energy component comes from the inner well and its oscillatory structure reflects the region of depleted photoionization amplitudes. In our previous publication,[19] the photoelectron spectra showed a strong peak at very low kinetic energy which arose from the wave packet in the region of its outside turning point for ΔT of 600 fs [see Figs. 4(a) and 4(b)]. In Fig. 8 this peak feature corresponds to $\Delta T=600$ fs. Such structure is noticeably lower relative to the strongest peak at earlier delay time. This is so because the kinetic energy distribution at an earlier delay time is essentially the same as that for the parallel case [$\theta_P=0$ case in Fig. 4(a)], while at $\Delta T=600$ fs there is significant contribution from the kinetic energy distribution for the perpendicular case [$\theta_P=\pi/2$ case in Fig. 4(b)] which is of considerably lower magnitude than the parallel case.

The effect of molecular rotation is more apparent in the photoelectron angular distributions (energy-integrated), i.e.,

$$A(\theta_k;\theta_R(\Delta T),\theta_P) = \int dk k^2 \int dR \left| \sum_{lm} \chi_{klm}(R,t_f;\theta_R(\Delta T),\theta_P) Y_{lm}(\theta_k,\phi_k) \right|^2 \tag{23}$$

than in the energy distributions of Fig. 8. Figure 9 shows these angular distributions (θ_k) in the XZ-plane ($\phi_k=0$) for pump photons of 3.600 eV (inner well) and 3.676 eV (top of barrier) and a probe photon of 2.278 eV. At short delay times the distributions are generally of the d_{z^2} type while near $\Delta T=1020$ fs, they show d_{xz} character. The angular distributions evolve between these extremes as the molecule rotates. The distributions for both the lower (inner well) and higher (top of barrier) pump photon energy cases show similar trends in their angular dependence (θ_k) but differ largely in their dependence on molecular rotation. This is due more to vibrational dynamics than rotational dynamics and arises from the dependence of the photoionization amplitudes on internuclear distance. The ion population varies widely as the wave packet moves through regions of changing photoionization amplitudes. To offset the effect of the varying ion signals, we show the angular distributions (θ_k) divided by the total ion signal for various $\theta_R(\Delta T)$ in Fig. 10. The resulting distributions are now quite similar for the lower and higher pump photon energies. The additional structure seen in the distributions for the higher pump photon energy when the molecule is almost perpendicular to the probe polarization reflects the higher l contributions to photoionization at the larger internuclear distances accessed by the wave packet. In either case the overall shape of these angular distributions gives an indication of molecular orientation relative to the probe laser and can be used to monitor molecular rotation.

C. Factorization of the vibrational and rotational contributions

These results show that dependence of the photoelectron angular distributions on molecular orientation can be potentially exploited to monitor molecular rotation. Such use of pump–probe photoelectron angular distributions for real-time mapping of rotation can be a valuable supplement to other techniques such as laser induced fluorescence (LIF).[23] However, even within the classical scheme, molecular rotation can introduce significant complexity in attempts to unravel the vibrational components of these photoelectron signals. It would hence be useful to isolate the vibrational contribution from such convoluted photoelectron spectra since the resultant spectra provide a window on vibrational

wave packets which can, in turn, be useful in analyzing ultrafast intramolecular dynamics. Here we explore an approach to isolating these vibrational contributions.

To begin, we assume that the photoelectron angular distributions are measured with respect to the probe field and that θ_P denotes the angle between the pump and probe polarization (see Fig. 2). The molecule is also assumed to rotate in a plane defined by the polarization vector of the pump and probe. Since the polarization vector of the probe can be decomposed into components parallel and perpendicular to the molecular axis, we may write:

$$\chi_{klm}(R,t_f;\theta_R(\Delta T),\theta_P) = \cos(\theta_R(\Delta T)-\theta_P)\chi_{klm}(R,t_f;\Delta T,0,0) + \sin(\theta_R(\Delta T)-\theta_P)\chi_{klm}\left(R,t_f;\Delta T,0,\frac{\pi}{2}\right), \tag{24}$$

where the first (second) term arises from the dipole component parallel (perpendicular) to the molecular axis. One can hence write the photoelectron angular distributions of Eq. (23) in the form

$$\begin{aligned} A(\theta_k;\theta_R(\Delta T),\theta_P) &= \cos^2(\theta_R(\Delta T)-\theta_P)A^{\parallel}(\theta_k;\Delta T)+\sin^2(\theta_R(\Delta T)-\theta_P) \\ &\quad\times A^{\perp}(\theta_k;\Delta T)+\cos(\theta_R(\Delta T)-\theta_P) \\ &\quad\times\sin(\theta_R(\Delta T)-\theta_P)[X] \\ &= \tfrac{1}{2}(A^{\parallel}(\theta_k;\Delta T)+A^{\perp}(\theta_k;\Delta T))+\tfrac{1}{2}\cos(2\theta_P) \\ &\quad\times[\cos(2\theta_R(\Delta T))(A^{\parallel}(\theta_k;\Delta T)-A^{\perp}(\theta_k;\Delta T)) \\ &\quad+\sin(2\theta_R(\Delta T))[X]]+\tfrac{1}{2}\sin(2\theta_P)[\sin(2\theta_R(\Delta T)) \\ &\quad\times(A^{\parallel}(\theta_k;\Delta T)-A^{\perp}(\theta_k;\Delta T))-\cos(2\theta_R(\Delta T))[X]], \end{aligned} \tag{25}$$

where

$$A^{\parallel}(\theta_k;\Delta T) = \int dk k^2 \int dR \left|\sum_{lm}\chi_{klm}(R,t_f;\Delta T,0,0)Y_{lm}(\theta_k,\phi_k)\right|^2, \tag{26}$$

$$A^{\perp}(\theta_k;\Delta T) = \int dk k^2 \int dR \left|\sum_{lm}\chi_{klm}\left(R,t_f;\Delta T,0,\frac{\pi}{2}\right)Y_{lm}(\theta_k,\phi_k)\right|^2, \tag{27}$$

and $[X]$ denotes a crossing term. Furthermore, defining

$$A_1(\Delta T)\equiv A^{\parallel}(\theta_k;\Delta T)+A^{\perp}(\theta_k;\Delta T), \tag{28}$$

$$A_2(\Delta T)\equiv\cos(2\theta_R(\Delta T))(A^{\parallel}(\theta_k;\Delta T)-A^{\perp}(\theta_k;\Delta T)) + \sin(2\theta_R(\Delta T))[X], \tag{29}$$

and

$$A_3(\Delta T)\equiv\sin(2\theta_R(\Delta T))(A^{\parallel}(\theta_k;\Delta T)-A^{\perp}(\theta_k;\Delta T)) - \cos(2\theta_R(\Delta T))[X], \tag{30}$$

Eq. (25) can be rewritten as

$$2A(\theta_k;\theta_R(\Delta T),\theta_P)=A_1(\Delta T)+\cos(2\theta_P)A_2(\Delta T) + \sin(2\theta_P)A_3(\Delta T). \tag{31}$$

Although $\theta_R(\Delta T)$ varies with the delay time ΔT, θ_P is known in advance. If measurements are carried out for three different θ_P's, say $\theta_P=0$, $\theta_P=\pi/4$, and $\theta_P=\pi/2$ and other parameters kept invariant, Eq. (31) yields three equations from which the unknowns, $A_1(\Delta T)$, $A_2(\Delta T)$, and $A_3(\Delta T)$ can be determined.

If the rotational time is known from other means, then $\theta_R(\Delta T)$ is simply given by $(2\pi/T_{rot})\Delta T$. One can then readily show from Eqs. (29) and (30) that

$$\cos(2\theta_R(\Delta T))A_2(\Delta T)+\sin(2\theta_R(\Delta T))A_3(\Delta T) = A^{\parallel}(\theta_k;\Delta T)-A^{\perp}(\theta_k;\Delta T)\equiv A_4(\Delta T). \tag{32}$$

The term $[X]$ can likewise be obtained from Eqs. (29) and (30). Combining Eqs. (28) and (32), we finally obtain

$$A^{\parallel}(\theta_k;\Delta T)=\tfrac{1}{2}(A_1(\Delta T)+A_4(\Delta T)) \tag{33}$$

and

$$A^{\perp}(\theta_k;\Delta T)=\tfrac{1}{2}(A_1(\Delta T)-A_4(\Delta T)). \tag{34}$$

Thus the photoelectron angular distributions for the probe polarization both parallel and perpendicular to the molecular axis can be obtained. Some examples of these photoelectron angular distributions are shown in Fig. 10 of Ref. 19. The procedure can be equally applied to obtain the photoelectron energy distributions $P^{\parallel}(\epsilon_k;\Delta T)$ and $P^{\perp}(\epsilon_k;\Delta T)$.

Although the above procedure permits deconvolution of the vibrational and rotational contributions to the photoelectron spectra, it is at best approximate since it neglects any dispersion of the rotational wave packets and effects due to Coriolis coupling between the vibrational and rotational motion. Furthermore, it assumes that all molecules are initially aligned with their molecular axis parallel to the pump polarization. Nonetheless, in the appropriate cases the procedure outlined above can provide a useful guide to extracting the photoelectron signals arising primarily from vibrational dynamics.

V. CONCLUDING REMARKS

We have incorporated a classical treatment of molecular rotation into our previously developed formulation of energy- and angle-resolved pump–probe photoelectron spectroscopy. The classical model should be primarily suitable for describing cases where the rotational motion is slow and where any coherent coupling in the rotational dynamics and between rotational and vibrational motion is weak. We have used energy- and angle-resolved pump–probe photoelectron spectra for wave packets on the $^1\Sigma_u^+$ double-minimum state of Na_2 to illustrate how such spectra are modified by rotational motion. As expected, these angle-resolved spectra are seen to depend quite sensitively on rotation. On the other hand, although the energy-resolved signals are less sensitive to rotation, the dependence of the photoionization amplitude on internuclear distance as the wave packet moves across the well results in an additional complex variation in the signals.

The procedure proposed here provides a useful approach for extracting the component of the signal arising primarily from the vibrational dynamics.

ACKNOWLEDGMENTS

This work has been supported by a grants from the Ministry of Education, Science, and Culture (Japan) and the National Science Foundation (U.S.).

APPENDIX

Rotation of the frame by the Euler angles $\hat{R}' = (\alpha, \beta, \gamma)$, $(0 \leqslant \alpha < 2\pi, 0 \leqslant \beta \leqslant \pi, 0 \leqslant \gamma < 2\pi)$ connecting the body frame to the probe frame in Eqs. (12) and (9) can be thought of as two Euler rotations in sequence, one from the body frame to the pump frame and one from the pump frame to the probe frame

$$\mathcal{D}(\alpha, \beta, \gamma) = \mathcal{D}(0, \theta_P, 0)\mathcal{D}(-\gamma_R, -\theta_R, -\phi_R). \tag{A1}$$

Here the angle γ_R is needed to unambiguously define the body frame with respect to the pump frame, but is arbitrary for the case of a linear molecule. Writing out the right hand side of Eq. (A1) as Cartesian rotation matrices and carrying out the multiplication results in a 3×3 matrix with matrix elements $\{a_{i,j} : i, j = 1,2,3\}$. Equating this with the Cartesian rotation matrix for the left hand side of Eq. (A1), β is determined as

$$\beta = \cos^{-1} a_{33}. \tag{A2}$$

Likewise α and γ are determined from the relations

$$(\cos\alpha, \sin\alpha) = \frac{(a_{31}, a_{32})}{\sin\beta} \tag{A3}$$

and

$$(\cos\gamma, \sin\gamma) = \frac{(-a_{13}, a_{23})}{\sin\beta}. \tag{A4}$$

When $\sin\beta = 0$, that is, if the probe polarization vector is parallel or antiparallel to the molecular axis, only one of (α, γ) is needed to represent the rotation about the Z-axis. In this case, taking $\gamma = 0$, α is determined from

$$(\cos\alpha, \sin\alpha) = a_{33}(a_{11}, a_{12}). \tag{A5}$$

[1] T. S. Rose, M. J. Rosker, and A. H. Zewail, J. Chem. Phys. **88**, 6672 (1988).
[2] A. H. Zewail, *Femtochemistry: Ultrafast Dynamics of the Chemical Bond* (World Scientific, Singapore, 1994), Vols. 1 and 2.
[3] *Femtochemistry*, edited by J. Manz and L. Wöste (VCH, Weinheim, 1995).
[4] *Chemical Reactions and Their Control on the Femtosecond Time Scale*, XXth Solvay Conference on Chemistry, edited by P. Gaspard, I. Burghard, I. Prigogine, and S. A. Rice, Adv. Chem. Phys., Vol. 101 (Wiley, New York, 1997).
[5] I. Fischer, D. M. Villeneuve, M. J. J. Vrakking, and A. Stolow, J. Chem. Phys. **102**, 5566 (1995); V. Blanchet, M. Z. Zgierski, T. Seideman, and A. Stolow, Nature (London) **401**, 52 (1999).
[6] A. Assion, M. Geisler, J. Helbing, V. Seyfried, and T. Baumert, Phys. Rev. A **54**, R4605 (1996).
[7] C. Jouvet, S. Martrenchard, D. Solgadi, C. Dedonder-Lardeux, M. Mons, G. Grégoire, I. Dimicoli, F. Piuzzi, J. P. Visticot, J. M. Mestdagh, P. D'Oliveira, P. Meynadier, and M. Perdrix, J. Phys. Chem. **101**, 2555 (1997).
[8] J. A. Davies, J. E. LeClaire, R. E. Continetti, and C. C. Hayden, J. Chem. Phys. **111**, 1 (1999).
[9] T. Baumert, J. L. Herek, and A. H. Zewail, J. Chem. Phys. **99**, 4430 (1993).
[10] T. Baumert and G. Gerber, Adv. At., Mol., Opt. Phys. **35**, 163 (1995).
[11] H. Ruppe, S. Rutz, E. Schneiber, and L. Wöste, Chem. Phys. Lett. **257**, 356 (1996).
[12] X. Song, C. W. Wilkerson, J. Lucio, S. Pauls, and J. P. Reilly, Chem. Phys. Lett. **174**, 377 (1990).
[13] M. R. Dobber, W. J. Buma, and C. A. de Lange, J. Chem. Phys. **99**, 836 (1993).
[14] J. A. Syage, Z. Phys. D: At., Mol. Clusters **30**, 1 (1994).
[15] T. Suzuki, L. Wang, and K. Kohguchi, J. Chem. Phys. **111**, 4859 (1999).
[16] M. Seel and W. Domcke, Chem. Phys. **151**, 59 (1991); M. Seel and W. Domcke, J. Chem. Phys. **95**, 7806 (1991).
[17] For example, Ch. Meier and V. Engel, Chem. Phys. Lett. **212**, 691 (1993); Ch. Meier and V. Engel, J. Chem. Phys. **101**, 2673 (1994); M. Braun, Ch. Meier, and V. Engel, *ibid.* **105**, 530 (1996).
[18] Y. Arasaki, K. Takatsuka, K. Wang, and V. McKoy, Chem. Phys. Lett. **302**, 363 (1999).
[19] Y. Arasaki, K. Takatsuka, K. Wang, and V. McKoy, J. Chem. Phys. **112**, 8871 (2000).
[20] Y. Arasaki, K. Takatsuka, K. Wang, and V. McKoy, J. Electron Spectrosc. Relat. Phenom. **108**, 89 (2000).
[21] K. Takatsuka, Y. Arasaki, K. Wang, and V. McKoy, Faraday Discuss. **115**, 1 (2000).
[22] R. R. Lucchese, G. Raseev, and V. McKoy, Phys. Rev. A **25**, 2572 (1982); R. R. Lucchese, K. Takatsuka, and V. McKoy, Phys. Rep. **131**, 147 (1986); K. Wang and V. McKoy, J. Chem. Phys. **95**, 4977 (1991).
[23] M. Dantus, R. M. Bowman, and A. H. Zewail, Nature (London) **343**, 737 (1990).